Electrochimica Acta 112 (2013) 686–691

Contents lists available at ScienceDirect

Electrochimica Acta

journal homepage: www.elsevier.com/locate/electacta

Electrooxidation of glycerol on platinum nanoparticles: Deciphering how the position of each carbon affects the oxidation pathways

Pablo S. Fernández[a], Cauê A. Martins[b], María E. Martins[a], Giuseppe A. Camara[b,*]

[a] Instituto de Investigaciones Fisicoquímicas Teóricas y Aplicadas (INIFTA), Facultad de Ciencias Exactas, UNLP, CCT La Plata-CONICET, 1900 La Plata, Argentina
[b] Institute of Chemistry/UFMS, C.P. 549, 79070-900 Campo Grande, MS, Brazil

ARTICLE INFO

Article history:
Received 13 July 2013
Received in revised form 3 September 2013
Accepted 5 September 2013
Available online xxx

Keywords:
Glycerol electrooxidation
In situ FTIR
Isotopically labeled glycerol
Platinum nanoparticles
Glyceraldehyde

ABSTRACT

In this work we investigate the electrooxidation of glycerol on platinum nanoparticles in acidic media. By using in situ FTIR and isotopically labeled glycerol ($^{13}CH_2OH—^{12}CHOH—^{13}CH_2OH$) we follow the reaction during a full cycle of oxidation and unravel the role of some important species on the electrooxidation pathways. Results indicate that terminal ($—^{13}CH_2OH$) and central ($—^{12}CHOH—$) groups are able to form adsorbed CO and that both contribute to the production of CO_2, although the terminal groups are easier to be oxidized than the central one, probably due to the steric effect provoked by $—^{13}CH_2OH$ which prevents the oxidation of $—^{12}CHOH—$. Moreover, glyceraldehyde seems to be an important intermediate for the generation of glyceric acid.

1. Introduction

The interest in the electrooxidation of glycerol has increased in the last few years, justified by the possibility to use this alcohol in direct alcohol fuel cells (DAFCs) [1–7] and as an intermediate for the production of valuable chemicals [8,9]. On this subject, an important aspect is the cheapening of glycerol on the worldwide market, caused by rising stocks of this substance, which is obtained as a side-product during the production of biodiesel at a mass ratio of 10% [9].

Recent papers have showed that the relative complexity of glycerol produces a myriad of products of incomplete oxidation, as well as species with partial cleavage of the carbon chain (i.e., 2-C species). For instance, in a recent paper of Koper et al., the authors have identified species containing two carbons (as glycolic acid) and one carbon (as formic acid) on Pt catalysts [8]. On the other hand, if the surface of the catalyst is modified by bismuth, dihydroxyacetone, glyceraldehyde and glyceric acid are mainly detected [8].

The paper of Koper et al. [8] reinforces the fact that the use of glycerol as a fuel in DAFCs requires the control of the electrooxidation pathways in order to improve the production of CO_2 (especially at low potentials) and maximize the deliverance of energy to the electrochemical interface. Such control is only possible if one has a good knowledge about the role of each superficial site on the electrooxidation of glycerol, which ultimately will provide the design of specific catalysts to promote the desired pathways.

In this context, in a recent paper we investigated the electrooxidation of glycerol on polycrystalline platinum by in situ FTIR spectroscopy [10]. By using isotopically labeled glycerol ($^{13}CH_2OH—CHOH—^{13}CH_2OH$) we were able to show that glycerol generates CO_2 from both types of carbons (i.e., the central one and the terminal ones), which implies that, at least to some extent, glycerol is able to completely dissociate on platinum surfaces [10].

However, the use of platinum in practical systems as DAFCs demands that the metal be used in form of nanoparticles (usually supported on carbon), and such systems are far more complex than polycrystalline platinum, mainly due to factors as different electronic density, particles with a wide range of diameters, several crystalline planes on the same particle and low coordination atoms, among others [11]. Hence, although the investigation on bulk electrodes is an important step to understand electrochemical reactions, the results obtained in such systems are not fully transferable to nanoparticles.

Herein, we take a step forward about the knowledge of glycerol electrooxidation on platinum surfaces. For that, we perform an in situ FTIR study with isotopically labeled glycerol on carbon-supported platinum nanoparticles.

Results reveal a complex mechanism in which glyceraldehyde seems to play a central role as an intermediate for the formation of glyceric acid. Moreover, FTIR shows that glycerol can be completely converted in CO during the early steps of adsorption, but the central

* Corresponding author. Tel.: +55 67 3345 3576; fax: +55 67 3345 3552.
E-mail address: giuseppe.silva@ufms.br (G.A. Camara).

0013-4686/$ – see front matter © 2013 Elsevier Ltd. All rights reserved.
http://dx.doi.org/10.1016/j.electacta.2013.09.032

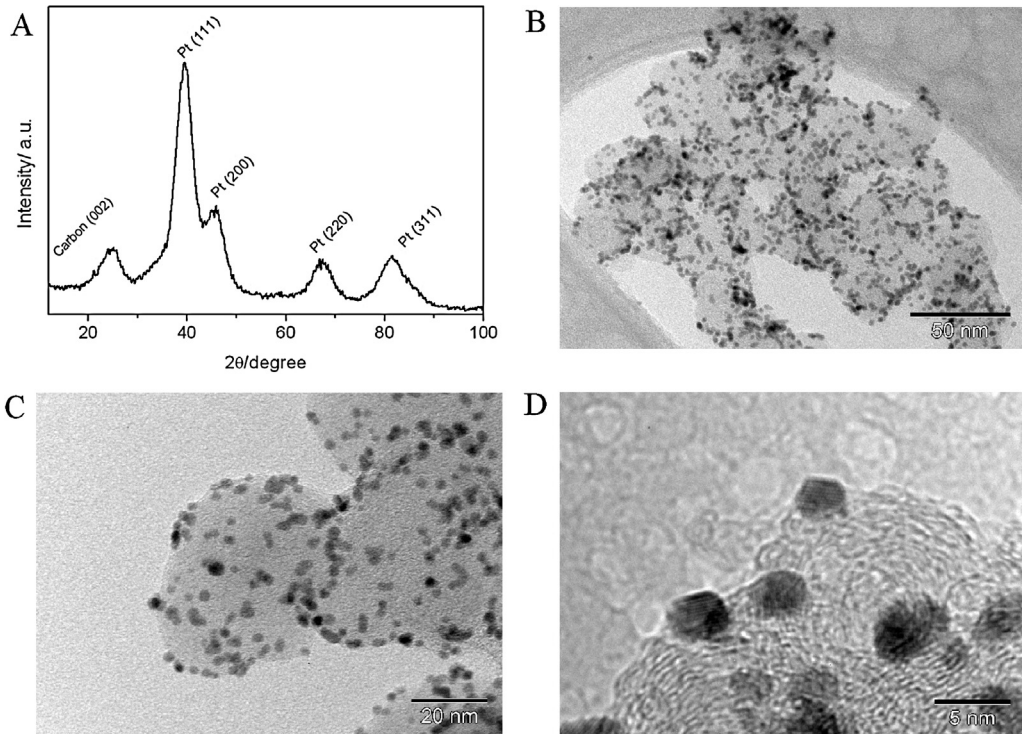

Fig. 1. Physical characterization of carbon supported platinum nanoparticles, consisting of A: XRD spectra. B, C and D refer to TEM images of different magnifications (the scale bars are indicated in the figures).

carbon (^{12}C) is somewhat shielded by its own carbon-chain and its oxidation only occurs after the terminal groups (^{13}C) have being oxidized.

2. Experimental

2.1. Synthesis of Pt/C catalysts

A typical method based on reduction of the precursor ions by polyols was used to prepare the Pt/C nanoparticles [12]. Shortly, Carbon Vulcan XC72R, polyvinylpyrrolidone (PVP-Aldrich) and a mixture containing ethylene glycol (EG – J. T. Baker) – water (3:1, v/v) were placed in a vessel and sonicated for 20 min to achieve a homogeneous dispersion. After, an aqueous solution containing 2 mmol dm^{-3} H_2PtCl_6 (Sigma–Aldrich) was added to the dispersion to obtain a platinum load of 40% (w/w) on the catalyst. Then, the mixture was sonicated for 10 min under continuous magnetic stirring and heated at 140 °C during one hour to allow the nucleation and growth of the metallic centers on the carbon support. The solution was then cooled at room temperature and finally centrifuged. The solid retained was thoroughly washed with Milli-Q® water and centrifuged again. This step was repeated five times. Afterwards, the remaining solid was dried at 70 °C for 2 days. The amount of PVP added to the solution was measured relative to the amount of Pt. The PVP monomer/Pt atom ratio was set to 0.3.

2.2. Working electrode preparation

Pt/C nanoparticles were deposited on a polycrystalline gold disk (10 mm of diameter) as follows: a Pt/C ink was prepared by adding 1 mg of the catalyst in a vessel with 25 μL of Nafion (Aldrich 5% v/v) and 2 mL of isopropanol. Then, the mixture was sonicated for 20 min. and an aliquot of 50 μL of this ink was applied on the gold substrate (kept at controlled temperature of 70 ± 2 °C). Once the deposit was completely dried, 50 μL of a diluted Nafion solution (90 μL of the original Nafion solution were diluted in 20 mL of methanol (Merck)) was applied onto the catalyst in order to form a film which protects the surface of the electrode, since during FTIR experiments it is pressed against a CaF_2 window.

2.3. Electrochemical testing

Pure N_2 was used to purge the solutions before and during the electrochemical experiments. Solutions were prepared with Milli-Q® water, (18.2 MΩ cm), $HClO_4$ (Merck, p.a.) and either normal or labeled glycerol (1,3-$^{13}C_2$ 99 atom % ^{13}C, Sigma–Aldrich). The counter electrode was a high area platinum ring. The electric potentials were measured against a reversible hydrogen reference electrode (RHE) in the same electrolyte and are presented in the same scale. All electrochemical runs were performed at 25 °C under oxygen-free conditions. In attempt to obtain a clean platinum surface, before each experiment, the working electrode was transferred to a three-compartment electrochemical cell containing 0.1 mol dm^{-3} $HClO_4$ and cyclic voltammetry experiments (20 cycles) were performed in the potential range comprised between 0.05 and 1.45 V at a sweep rate of 20 mV s^{-1}, according to a procedure recently proposed by us [13].

2.4. In situ FTIR experiments

FTIR experiments were carried out using an AUTOLAB (Model PGSTAT 128N) potentiostat coupled to a MB-100 spectrometer (Bomem) with a MCT detector. The cell used for these experiments is described in detail elsewhere [14]. The electrochemical cell was fitted to a CaF_2 planar window. Reflectance spectra were collected in the presence of 0.255 mol dm^{-3} glycerol + 0.1 mol dm^{-3} $HClO_4$, being calculated as the ratio (R:Ro), where R represents a spectrum at a given potential and Ro is the spectrum collected at 0.12 V. Positive-and-negative going bands represent, respectively, loss and gain of species at the sampling potential. Spectra were computed

from an average of 50 interferograms. The spectral resolution was set to 4 cm^{-1}. The potential was first kept at 0.12 V while 0.255 mol dm^{-3} normal or isotopically labeled glycerol was admitted to the cell, subsequently shifting to the starting potential up to 0.15 V with 0.05 V potential steps being applied. Each potential was kept during 80 s while 50 interferograms were collected.

2.5. Physical characterization of Pt/C catalysts

XRD patterns of the samples were obtained using the Cu Kα radiation in a Rigaku Multiflex equipment. Diffraction data were collected by step scanning with a step size of 0.02° in the range of 5–90°, with an interval of 2 s between steps.

Morphological information of the catalysts (particle size and distribution) was obtained via transmission electron microscopy (TEM) using a Carl Zeiss CEM 902 apparatus with a Proscan high-speed slow-scan CCD camera and digitalized (1024 × 1024 pixels, 8 bit) using the AnalySis Software. The particle size distributions were determined by measuring the nanoparticles from micrographs using Image J 1.44p Software.

3. Results and discussion

3.1. Physical characterization

Fig. 1 shows the XRD diffractograms of Pt/C (Fig. 1A) and TEM images of the nanoparticles in three scales (Fig. 1B–D). The diffraction peak at ~26° is due to the (0 0 2) plane of the hexagonal structure of carbon Vulcan® XC72R. The additional diffraction peaks at around 39, 46, 67 and 82° are due to diffractions of Pt (1 1 1), (2 0 0), (2 2 0), and (3 1 1) planes, respectively, of the typical Pt face centered cubic (fcc) phase. Average crystallite size was calculated using the Scherrer formula for each reflection. The average crystallite size was of 2.5 ± 0.2 nm. These results corroborate the mean particle size estimated from TEM images (2.74 ± 0.04 nm) and suggest that most particles are formed by single crystals. Fig. 1B–D shows that the Pt NPs (dark spots) are fairly dispersed on the carbon support (brighter region). Moreover, Fig. 1C makes clear that most particles present a homogeneous size and are spherical. The lattice spacing estimated from some nanoparticles like the ones in Fig. 1D was 0.23 nm.

After being characterized, the supported nanoparticles were used as electrocatalysts for glycerol electrooxidation. Results are presented and discussed in next section.

3.2. Electrooxidation of isotopically labeled glycerol followed by in situ FTIR

Fig. 2A shows some selected spectra recorded in presence of 0.255 mol dm^{-3} labeled glycerol (LG) and 0.1 mol dm^{-3} $HClO_4$ during an up-going polarization curve. The first feature apparent in the spectra is a little negative band at ~2040 cm^{-1}, relative to CO adsorbed in an on-top configuration [6], which begins to develop at 0.15 V. This band grows up to 0.65 V and indicates that the central carbon of glycerol has been detached from the molecule during the adsorption steps. Starting from this observation, it will be expected that the signal referring to ^{13}CO (i.e., CO formed from the dissociation of terminal $-^{13}CH_2OH$ groups) be twice more intense than the corresponding to ^{12}CO. However, Fig. 2B shows the band of ^{13}CO (located at 1990 cm^{-1}) is far less intense than the ^{12}CO band. The low intensity of the ^{13}CO band is probably caused by a dipole coupling which causes the lowering of its signal and the dominance of ^{12}CO [15,16]. Such coupling makes impracticable to use CO bands for quantitative purposes, but despite this limitation, the signals showed in Fig. 2B are still relevant, since, for the first time, they demonstrate the ability of platinum nanoparticles

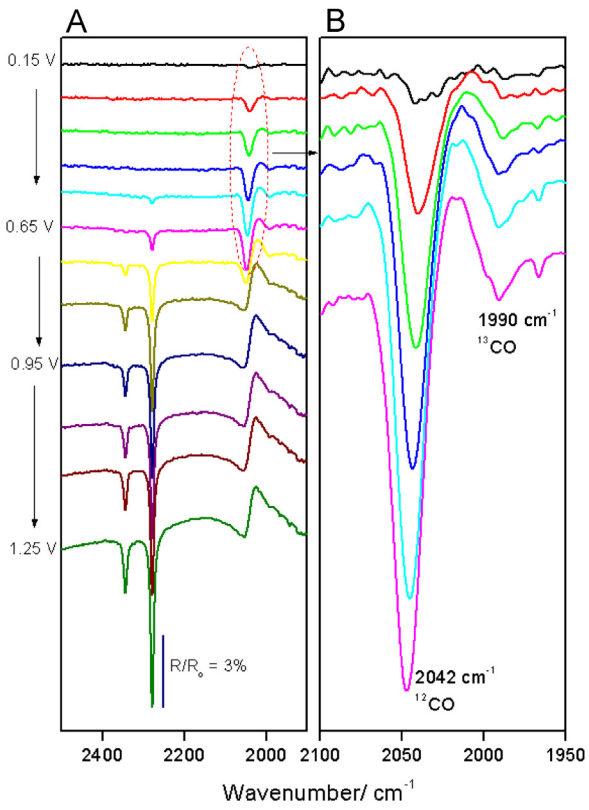

Fig. 2. (A) in situ FTIR spectra for Pt/C nanoparticles supported on gold at different potentials (indicated) in the presence of 0.255 mol dm^{-3} labeled glycerol + 0.1 mol dm^{-3} $HClO_4$. Reference spectra taken at 0.12 V. Sample spectra: 50 interferometer scans measured after applying successive potential steps of 0.05 V. (B) Details of both CO bands in the potential range of 0.15–0.65 V.

to cleave glycerol molecules, and corroborate previous observations made by us on polycrystalline platinum surfaces [10]. Summarizing, Fig. 2B unequivocally indicate that both types of carbon (terminal and central ones) are able to produce CO as an intermediate of glycerol electrooxidation.

Other features of Fig. 2A are the bands located at 2343 and 2278 cm^{-1}, relative to the production of $^{12}CO_2$ and $^{13}CO_2$, respectively [10]. The $^{13}CO_2$ band starts to grow at 0.45 V while the $^{12}CO_2$ only becomes discernible at 0.75 V. This result suggests that the formation of CO_2 from terminal groups is easier than from the central one. Furthermore, it is worth noting that the $^{13}CO_2$ band is significantly more developed that the $^{12}CO_2$ band at long of the whole potential range. Indeed, the dominance of the $^{13}CO_2$ band is expected since LG ($^{13}CH_2OH$—$^{12}CHOH$—$^{13}CH_2OH$) has two ^{13}C for each ^{12}C. However, the ratio $^{13}CO_2/^{12}CO_2$ (not shown) is always bigger than two, which suggests that $^{13}CO_2$ is easier to be formed than $^{12}CO_2$.

Aiming to follow the behavior of the CO band in major details, we performed a new experiment in presence of a regular glycerol solution of same concentration. The choice was made in order to maximize the signal of CO, since the usage of labeled glycerol splits the band in two features, as showed in Fig. 2. Some selected spectra obtained during a complete cycle are presented in Fig. 3.

Fig. 3 shows that the CO band is well-developed at 0.35 V (it arises at 0.15 V) and grows up to 0.55 V. After that, CO is consumed to form CO_2 and the corresponding band decreases. During the reverse scan, the CO band becomes visible again (although as minor feature) at 0.85 V, which coincides with the resumption of production of CO_2 (as will be showed in Fig. 5). Then, the CO band grows up to the end of the experiment, while the formation of CO_2 ceases at low potentials. This profile corroborates the assumption that a

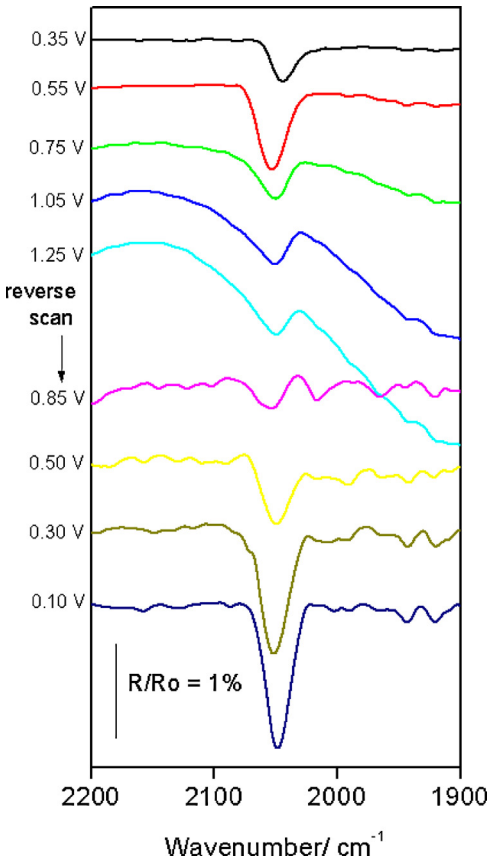

Fig. 3. Details of the CO band on Pt/C nanoparticles supported on gold collected during a full scan (potentials indicated) in 0.255 mol dm^{-3} glycerol + 0.1 mol dm^{-3} $HClO_4$. Experimental conditions as in Fig. 2.

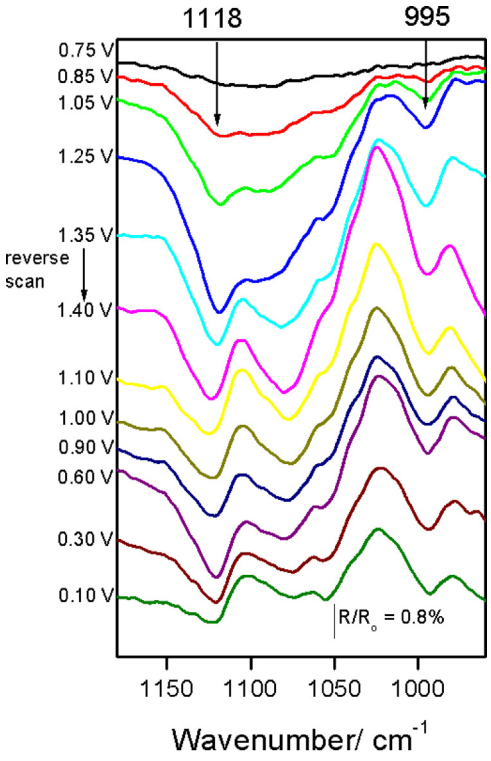

Fig. 4. (A) Detail of in situ FTIR spectra in the wavenumber range of 1200–950 cm^{-1} obtained at different potentials (indicated) in presence of 0.255 mol dm^{-3} labeled glycerol + 0.1 mol dm^{-3} $HClO_4$. Experimental conditions as in Fig. 2.

step that involves the co-adsorption of CO and Pt-OH occurs during both sweeps. Further details about the behavior of CO with the potential will be given later.

In order to inspect the formation of other substances, we show the details of selected spectra in the region of 1200–950 cm^{-1} during a full cycle of oxidation in Fig. 4. Here is important to note that owing to the relative low concentration of glycerol used in this work, bands associated to all other species than CO and CO_2 present very low intensity. Hence, we decided to isolate this region from the spectra showed in Fig. 2A since the magnitudes of the band are quite different.

Fig. 4 shows two features at 1118 and 995 cm^{-1}. Taking into account that the presence of ^{13}C lowers the wavenumber of any functional group which contains terminal carbons, we assume that these bands correspond to a C—O stretching of glyceraldehyde and to a C—C—O asymmetric stretching of glyceric acid, respectively, based on references [17] and [18]. Moreover, the whole region seems to be superimposed by a wide band, probably due to a Cl—O stretching form perchlorate [14]. This wide signal makes the estimation of area of both bands in Fig. 4 impractical. Due to this limitation, we tentatively used the height of the peaks for both signals as a possible way to follow their development with the potential. The corresponding results (and the band intensity areas for CO, $^{13}CO_2$ and $^{12}CO_2$) were normalized by their respective maximum (so they are presented in a common scale) and are presented in Fig. 5.

For purposes of visualization, the different signals were separated in Fig. 5A and B. Following the evolution of the system with the potential, we describe and discuss the behavior of each band as a function of the several potential ranges investigated. The direction of the potential scan is indicated by arrows (→ and ← represent upward and downward scans, respectively).

0.15 → 0.40 V. The only signal emerging is the CO band, which probably means that during the early stages of adsorption, some glycerol molecules are cleaved and CO accumulates on the surface up to 0.4 V (Fig. 5A).

0.40 → 0.60 V. CO begins to be oxidized and little amounts of $^{13}CO_2$ are formed, but the band of CO is still growing, indicating that the oxidation step is sluggish compared to the dissociative adsorption (Fig. 5A). $^{13}CO_2$ begins to be produced earlier than $^{12}CO_2$.

0.60 → 0.75 V. $^{12}CO_2$ is formed (Fig. 5A), probably because part of the surrounding CO (^{13}CO, not discernible here) was oxidized, leaving sites able to adsorb water. According to previous works, the CO_2 generated at low potentials seems to originate mainly from the oxidation of CO through a Langmuir–Hinshelwood (L-H) step [6,17]. Hence, we can state that the oxidation of glycerol begins by the terminal groups (^{13}C) and reaches the core carbon (^{12}C) only after the terminal ones have being oxidized.

0.75 → 1.20 V. The CO signal decreases sensibly, but a remaining bipolar band can still be perceived at high potentials. However, the very low intensity of this band (see Fig. 3) and its distorted shape make difficult to perform a quantitative analysis. After the decreasing of the CO signal, the formation of $^{13}CO_2$ and $^{12}CO_2$ slows down and reach a narrow plateau around 0.9 V. Interestingly, more $^{13}CO_2$ is proportionally produced in this potential range (remembering that both signals were normalized in such a way that their maxima coincide). Assuming a L-H step, the easier production of $^{13}CO_2$ is explained by a favorable position of the terminal groups to react with Pt-OH species, while the central fragment is surrounded by two terminal groups that can impose some steric effect [6]. At 0.75 V glyceraldehyde and glyceric acid begin to be detected (Fig. 5B) but is possible that glyceraldehyde has

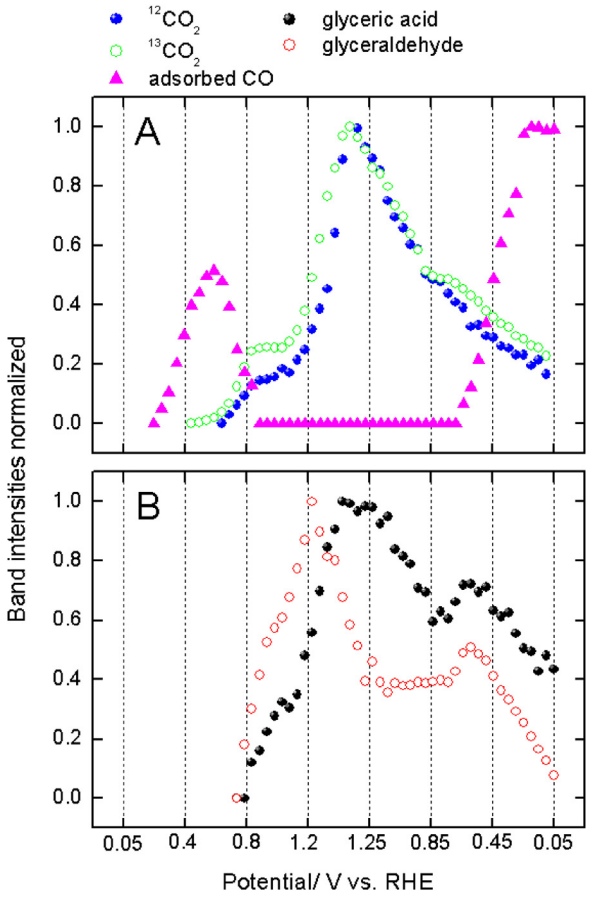

Fig. 5. Band intensities as a function of the potential in presence of 0.255 mol dm^{-3} labeled glycerol + 0.1 mol dm^{-3} $HClO_4$ on Pt/C nanoparticles. Signals refer to (A) $^{13}CO_2$, $^{12}CO_2$ and CO; (B) glyceric acid and glyceraldehyde. Data extracted from spectra like those shown in Figs. 2–4. The symbols corresponding to each species are indicated in the figure.

been formed at lower potentials, while its band remained hidden by the Cl—O signal which appears in the same region. Interestingly, glyceraldehyde signal grows faster than the glyceric acid corresponding band, probably because its formation is a facile step which involves the exit of two H-atoms.

0.90 → 1.45 V. Here the system enters a new regime of oxidation. Soon after glyceraldehyde is detected, the signal corresponding to glyceric acid grows up at similar rate. This observation suggests that glyceraldehyde could be an intermediate of glyceric acid. Moreover, conversely to the previous situation, the second wave of formation of CO_2 is tentatively explained in terms of an oxidation pathway through an Eley–Rideal step [6], in which these species do not need to be adsorbed on the surface to react with Pt-OH. In this situation, the relative position of the carbon atom in the molecule seems to exert a weaker influence on its reactivity and the pathway leading to $^{12}CO_2$ is less affected than in the previous case. Although glyceraldehyde can also be an intermediate of the formation of CO_2, the mere inspection of the signals in Fig. 5 does not allow reaching a conclusion.

1.25 ← 1.45 V. At these high potentials the interaction of water with the surface is probably too strong to allow that the adsorption of glycerol molecules (or its residues) be preferential. Then, all the oxidation pathways seem to be inhibited. As a consequence, band intensities of glyceric acid (Fig. 5B), $^{13}CO_2$ and $^{12}CO_2$ (Fig. 5A) start to decrease at similar rates, which merely indicates that their production rates are not enough to replenish them inside the thin layer.

0.85 ← 1.25 V. The change in the slope of the glyceraldehyde band intensity suggests that its production becomes faster than its consumption. An E-R step is probably operative in this potential range.

0.55 ← 0.85 V. Short after the formation of glyceraldehyde is enhanced, bands relative to $^{13}CO_2$ (Fig. 5A) and glyceric acid (Fig. 5B) start to grow again. The glyceraldehyde signal grows up to 0.55 V. At this potential range the surface is enough positive to allow the release of protons, but there is no much water adsorbed to feed the CO_2 pathways, which are more oxygen demanding than the glyceric acid pathway. Consequently, only a little inflection point is observed for $^{13}CO_2$ (i.e., some $^{13}CO_2$ is still formed, but in minor amounts) while the glyceric acid pathway is resumed. Furthermore, the dissociation of glyceraldehyde (or glycerol itself) and the lack of superficial water at these low potentials provoke a new accumulation of CO on the surface and its signal starts to grow again.

0.05 ← 0.55 V. The potential is too low to promote any oxidation pathway. Consequently, CO accumulates on the surface while all the other band intensities show the decrease characteristic of the low diffusion of the species outside the thin layer.

A last point that demands analysis is the fact that the magnitudes of the CO band are higher during the backward scan than at the beginning of the sweep. Here, is important to keep in mind that the production of CO occurs in different surface conditions during a full cycle. In the direct scan, CO is formed from glycerol at low potentials, where probably there is still some hydrogen adsorbed. Also, glycerol molecules can be adsorbed without cleavage, generating glyceraldehyde among other species. Hence, part of the surface becomes recovered by other species than CO. When these species are oxidized at high potentials, they leave the surface and release sites able to adsorption. Finally, when the potential sweep is reverse there is plenty of superficial sites which can accommodate intact molecules and promote the cleavage in such a way that 1-C species can be adsorbed, thus recovering the surface by CO.

The results discussed here illustrate the power of FTIR to monitor, in situ, the oxidation pathways of glycerol. However, the knowledge about some important steps is still fragmentary (e.g. the structure of adsorbed intermediates) and should be pursued in future works.

Finally, this paper shows that Pt NPs are able to completely break the glycerol molecule at very low potentials. However, as happens with many organic molecules possessing small chains, an important amount of reactive oxygenated species (for example, Pt-OH) is necessary to efficiently oxidize the residues. Therefore, the design of new, optimized catalysts, requires the development of Pt-M alloys, where M is a metal (or metal oxide) able to generate oxygenated species more easily than Pt, thus anticipating the oxidation steps.

4. Conclusions

- Terminal (—$^{13}CH_2OH$) and central (—$^{12}CHOH$—) groups of glycerol form adsorbed CO at low potentials, indicating that, at least to some extent, glycerol is able to completely dissociate on Pt nanoparticles.
- The electrooxidation of isotopically labeled glycerol generates both $^{13}CO_2$ and $^{12}CO_2$, but the oxidation of the terminal —$^{13}CH_2OH$ groups seems to be easier than that of the central group. Consequently, $^{13}CO_2$ is responsible for the major contributions for the production of CO_2 in the whole range of potentials.
- At intermediary potentials the formation of $^{13}CO_2$ seems to be favored through a L-H mechanism. Conversely, at high potentials CO_2 is formed from both groups at similar rates.

- After the consumption of CO the system enters a new regime of oxidation, in which glyceraldehyde seems to be an intermediate for the production of glyceric acid.
- During the reverse sweep, the oxidation of glycerol is resumed, mainly due to the formation of glyceraldehyde, glyceric acid and CO.

Acknowledgements

The authors acknowledge financial assistance from CNPq (Grant # 554591/2010-3), FUNDECT (Grants # 23/200.178/2010 and # 23/200.583/2012), CAPES, MINCyT and FINEP. P.S. Fernández is indebted to CONICET (Consejo Nacional de Investigaciones Científicas y Técnicas) for a fellowship. C.A. Martins thanks CNPq for a fellowship (Grant # 140426/2011-6).

References

[1] R.S. Ferreira Jr., M.J. Giz, G.A. Camara, Influence of the local pH on the electrooxidation of glycerol on palladium–rhodium electrodeposits, Journal of Electroanalytical Chemistry 697 (2013) 15.
[2] M. Simões, S. Baranton, C. Coutanceau, Electro-oxidation of glycerol at Pd based nano-catalysts for an application in alkaline fuel cells for chemicals and energy cogeneration, Applied Catalysis B: Environmental 93 (2010) 354.
[3] Y. Holade, C. Morais, S. Arrii-Clacens, K. Servat, T.W. Napporn, K.B. Kokoh, New preparation of PdNi/C and PdAg/C nanocatalysts for glycerol electrooxidation in alkaline medium, Electrocatalysis (2013) (in press).
[4] M. Simões, S. Baranton, C. Coutanceau, Electrochemical valorisation of glycerol, ChemSusChem 5 (2012) 2106.
[5] A. Falase, M. Main, K. Garcia, A. Serov, C. Lau, P. Atanassov, Electrooxidation of ethylene glycol and glycerol by platinum-based binary and ternary nanostructured catalysts, Electrochimica Acta 66 (2012) 295.
[6] J.F. Gomes, C.A. Martins, M.J. Giz, G. Tremiliosi-Filho, G.A. Camara, Insights into the adsorption and electro-oxidation of glycerol: self-inhibition and concentration effects, Journal of Catalysis 301 (2013) 154.
[7] J.F. Gomes, F.B.C. de Paula, L.H.S. Gasparotto, G. Tremiliosi-Filho, The influence of the Pt crystalline surface orientation on the glycerol electro-oxidation in acidic media, Electrochimica Acta 76 (2012) 88.
[8] Y. Kwon, Y. Birdja, I. Spanos, P. Rodriguez, M.T.M. Koper, Highly selective electro-oxidation of glycerol to dihydroxyacetone on platinum in the presence of bismuth, ACS Catalysis 2 (2012) 759.
[9] M. Pagliaro, R. Ciriminna, H. Kimura, M. Rossi, C. Della Pina, From glycerol to value-added products, Angewandte Chemie International Edition 46 (2007) 4434.
[10] P.S. Fernández, M.E. Martins, C.A. Martins, G.A. Camara, The electro-oxidation of isotopically labeled glycerol on platinum: new information on C—C bond cleavage and CO_2 production, Electrochemistry Communications 15 (2012) 14.
[11] F. Maillard, E.R. Savinova, P.A. Simonov, V.I. Zaikovskii, U. Stimming, Infrared spectroscopic study of CO adsorption and electro-oxidation on carbon-supported Pt nanoparticles: interparticle versus intraparticle heterogeneity, Journal of Physical Chemistry B 108 (2004) 17893.
[12] M. Chen, Y. Xing, Polymer-mediated synthesis of highly dispersed Pt nanoparticles on carbon black, Langmuir 21 (2005) 9334.
[13] P.S. Fernández, D.S. Ferreira, C.A. Martins, H.E. Troiani, G.A. Camara, M.E. Martins, Platinum nanoparticles produced by EG/PVP method: the effect of cleaning on the electrooxidation of glycerol, Electrochimica Acta 98 (2013) 25.
[14] T. Iwasita, F.C. Nart, In situ infrared spectroscopy at electrochemical interfaces, Progress in Surface Science 55 (1997) 271.
[15] J.J. Shin, W.J. Tornquist, C. Korzeniewski, C.S. Hoaglund, Elementary steps in the oxidation and dissociative chemisorption of ethanol on smooth and stepped surface planes of platinum electrodes, Surface Science 364 (1996) 122.
[16] P. Hollins, J. Pritchard, Infrared studies of chemisorbed layers on single crystals, Progress in Surface Science 19 (1985) 275.
[17] C.A. Martins, M.J. Giz, G.A. Camara, Generation of carbon dioxide from glycerol: evidences of massive production on polycrystalline platinum, Electrochimica Acta 56 (2011) 4549.
[18] P.S. Fernández, M.E. Martins, G.A. Camara, New insights about the electro-oxidation of glycerol on platinum nanoparticles supported on multi-walled carbon nanotubes, Electrochimica Acta 66 (2012) 180.